Experimental protocols for the understanding of accelerated degradation and diagnosis of a proton exchange membrane electrolyser

Edwin URBANO[1,2], Elodie PAHON[1], Nadia YOUSFI STEINER[1] and Melaine GUILLOU[2]

***Abstract*— Proton exchange membrane electrolysers are undoubtedly one of the most promising technologies for coupling with renewable energies. However, significant improvements in lifetime and production costs must be achieved before they can be applied on a large scale. Experimental protocols that allow the diagnosis and assessment of degradation, on timescales considerably shorter than the expected lifetime, are of great interest among industries and the scientific community. This work then proposes an experimental protocol aimed at studying degradation under stress conditions.The protocol was implemented in two different configurations: single cell and short stack, with diagnostic periods including a steady-state polarization curve and impedance spectroscopy, both in galvanostatic mode. With a degradation rate of 36.5 uV/h/cell for the single cell and 18 uV/h/cell for the short stack, the experiments show in both cases that: temperature has a very significant effect on the degradation of the cathode catalyst, very low frequency current cycling regenerates the electrochemical conditions, high current densities are the most punishing, and a large proportion of the losses can be recovered with a suitable rest period. Three peaks have been identified in the DRT analysis: P1, mass transport phenomena and P2 + P3 oxygen evolution reaction, charge and proton transport.**

I. INTRODUCTION

Proton exchange membrane (PEM) electrolysers can produce high purity hydrogen, offering high efficiency and fast response times, making them ideal for coupling with renewable energy sources [1]. However, long-term durability must be improved before large-scale industrial application, as degradation mechanisms can significantly influence efficiency and technology lifetime [2]. Understanding and diagnosing such degradation mechanisms is therefore the key to improving reliability and reducing global costs.

Accelerated testing protocols have been widely used in fuel cells to predict long-term degradation over shorter periods of time. For electrolysers, the application of these protocols has been less explored [3]. These protocols should make it possible to identify and analyse degradation phenomena such as catalyst dissolution, metal oxidation, membrane thinning and increased interfacial resistance. For the validation of these protocols, it is essential to correlate the observed phenomena with real-world operating conditions and to assess their impact on performance indicators such as overpotential evolution, impedance changes and gas production efficiency [4].

The main reviews on the degradation of PEM electrolyzers by [5] and [6] focus on their materials and components; nevertheless, the relationships with real operating conditions are not very recurrent in the explored studies. Experimental studies and the availability of data that allow a proper analysis of known degradation phenomena and the diagnosis of the state of health of the technology are also rather scarce. From the literature review carried out by these authors, presented in [7], it can be stated that degradation phenomena are intrinsically linked to the electrolyser components and their materials or to the interaction between several of them. In a general classification, degradation can be attributed to chemical, mechanical and environmental factors. Table I summarises, from [7], the degradation phenomena associated with each of the cell components and the stress factors identified.

This study presents an experimental framework for the evaluation of the accelerated degradation of a PEM electrolyser, based on the hypotheses put forward in the literature. The experimental protocols are applied to two different configurations: single cell and 10-cell stack, and combine in-situ electrochemical characterisation tests, such as polarisation curve analysis (I/V) and electrochemical impedance spectroscopy (EIS), as diagnostic tools. These protocols are the result of the analysis of accelerated degradation studies presented in [7]. By systematically analysing degradation trends, it is expected to establish a methodology for the lifetime prediction and the design of accelerated stress test protocols (AST) adapted to real operating conditions.

Following the analysis of degradation phenomena, current density, voltage, temperature, pressure, flow rate and water quality have a direct impact on one or more of the phenomena (Table I). In order to analyse these relationships and to understand how to accelerate the degradation phenomena, the following sections present an experimental protocol focusing on the effects of current/voltage and temperature as stress factors, with constant reagent pressure and water flow rate. To diagnose the degradation modes, the overpotential evolutions, through I/V analysis, and reconstruction of equivalent circuits and relaxation time distributions from EIS measurements. These principles are also introduced in the following sections.

II. BASICS OF ELECTROCHEMICAL IMPEDANCE SPECTROSCOPY ANALYSIS

Electrochemical impedance spectroscopy (EIS) is a fundamental tool for the diagnosis of electrochemical systems, such as batteries and PEM fuel cells and electrolysers. This non-destructive method allows the identification of different frequency-dependent electrochemical processes such as

[1]Université Marie et Louis Pasteur, UTBM, CNRS, institut FEMTO-ST, F-90000 Belfort, France edwin.urban-castano@utbm.fr

[2]Direction Opérationnelle Recherche et Developpement, Michelin Ladoux, Cébazat, France

TABLE I: Overview of PEM electrolyser degradation phenomena

Component	Category	Phenomena	Stress Factor
Polymer Membrane	Chemical	Radical attack	Current Temperature
		Inhibition by impurities	Water quality
	Mechanical	Mechanical stress	Clamping force
		Hydraulic pressure	Water flow
	Hydrothermal	Swelling & Thinning	Water flow Temperature
Catalyst	Chemical	Catalyst dissolution	Current Temperature
		Agglomeration & migration	Current Temperature
		Ion contamination	Water quality
		Support passivation	Current Temperature
Bipolar Plates Diffusion Layers	Chemical	Passivation (Ti/Stainless steel)	Current Temperature
		Hydrogen embrittlement	Current Temperature
	Mechanical	Mechanical stress	Clamping force

ion/charge transfer, catalyst reactions, double layer effect and mass transport [8], [9]. This section presents the basis for the subsequent analysis of the relaxation time distribution (DRT) as a model-free method, from the EIS data. Electrical circuit modelling (ECM) is also introduced, supporting the first approach.

To avoid interference from non-steady and non-linear data, validation is a fundamental step. Good data quality and high signal-to-noise ratio is essential, especially for the DRT method, where even small deviations or impressions at the measurement points can lead to misinterpretation [10]. The Kramers-Kronig (KK) transform guarantees for the impedance data set that if the real and imaginary parts satisfy the given constraints (see [9]), the analysed impedance data satisfies the linearity and time invariance conditions. As the resolution of the semi-infinite integral of the transform is not possible analytically, in practice the validity test is modified so that a measurement model satisfying the KK transform is fitted to the experimental data and the residuals are analysed. For this work, the linearity test proposed in [11] is applied and it is considered that if the relative residuals are less than $\pm 2\%$ over the entire measurement frequency window, the data satisfy the linearity and time invariance condition.

A. DISTRIBUTION OF RELAXATION TIME

Usually, an ECM is employed for the EIS analysis, however, this method requires preliminary system information. On the other hand, the DRT method allows the identification and deconvolution of the polarisation phenomena on the basis of the characteristic time constants, without the need for prior knowledge of the system.

A series connection of RC elements and a resistor can emulate the capacitive response of a system. Based on this principle, the DRT method distributes the RC element resistance scores on their related time constants. The deconvolution of the impedance spectrum in a DRT exhibits the processes with close time constants by having a higher resolution in the frequency domain [12]. The relationship between the impedance $Z(\omega)$ and the distribution function $g(\tau)$ satisfies (1), that also satisfies the boundary condition expressed in (2) [13].

$$Z(\omega) = R_0 + R_{pol} \int_0^\infty \frac{g(\tau)}{1 + j\omega\tau} d\tau \tag{1}$$

$$\int_0^\infty g(\tau) d\tau = 1 \tag{2}$$

where, R_0 denotes ohmic resistance in the circuit and R_{pol} the polarisation resistances of the impedance.

The DRT calculation generally employs a numerical approach using a fit-based adjustment, stabilised by Tikhonov regularisation [14]. Choosing the right regularisation value for the DRT calculation is challenging, because very low parameters can lead to an overestimation of the number of processes and high values may not separate processes with close time constants. In the studies consulted, the value is generally 0.01, 0.001 or 0.005 for PEM electrolysers [10], [12], [13]. Our study is based on the work developed by [16] and [17] for the resolution of the DRT method, so we have applied a Gaussian discretisation method with a lambda of 0.001 where the trade-off between smoothness and sensitivity to measurements is the best. Each of the peaks obtained by peak analysis can then be associated with an electrochemical phenomenon and supported by the resolution of the corresponding electric circuit model [18].

B. EQUIVALENT CIRCUIT MODELLING

To extract meaningful parameters from the EIS data, *ECM* is used through a combination of resistive, capacitive and diffusive elements that simulate the electrochemical behaviour of the system. The *ECM* must then be able to emulate the different voltage drops produced when the electrolyser is in operation [15]. The general cell voltage equation is given by (3) and it able to represent the electrical circuit as shown in Figure 1. Where total cell voltage can be computed from individuals elements sum, representing reversible voltage and losses.

$$E_{cell} = E_{rev} + E_{ohm} + E_{act} + E_{diff} \tag{3}$$

From the general circuit given in Figure 1 different circuit models can be established depending on the assumptions made. This gives a good estimate of the process caused by voltage drops across a set of electrical circuit elements. In addition to the ohmic and reversible voltage drop, generally identifiable with polarisation curves (discussed in the results),

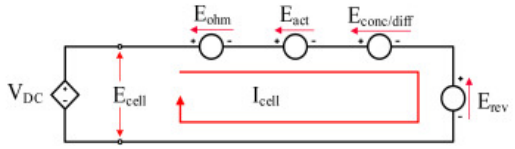

Fig. 1: Electrical circuit representing a PEM cell [15]

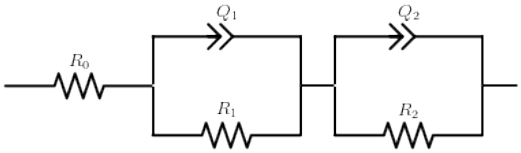

Fig. 2: Electrical circuit model for a PEM electrolyser cell.

the double layer capacitance effect also needs to be considered. This effect is due to the accumulation of charges on both sides of the membrane and bases its influence on the activation and concentration over-voltage.

The charges accumulation on the membrane surfaces together with the opposite type of charge on the surface of the electrodes then generates a capacitive effect. In the ECM this effect can be emulated with the use of a condenser element. Elements to which a parallel resistor is added for voltage drop emulation. The double layer effect voltage drop, combined with the capacitive effect, is represented by an *RC* branch. A simple ECM for an electrolyser cell is therefore generally composed of a resistor (R_{ohm}) associated in series with several *RC* element representing activation and charge/ion transport phenomena. For high current intensities, an RC_{diff} element or a Warburg (W) element can be associated in series to represent the diffusive effects, not considered in this work.

The actual impedance measurements, however, cannot be represented precisely by a perfect capacitive element. For high frequencies the inductive wire effects are also present in our results. Therefore, the *ECM* used in this work employs constant phase elements (*CPE*) to emulate imperfect capacitors. The *ECM* proposed is given in Figure 2, composed of a resistor, R_0, in series connection with two *RC* elements, representing the ohmic resistance, the activation and the mass transport phenomena, respectively. The quantification of the elements is performed by the impedance curve fitting which is reconstructed through (4) for the validation of the *ECM*.

$$Z(j\omega) = R_{ohm} + Z_1 + Z_2 \tag{4}$$

where, Z is the complex impedance, R_{ohm}, ohms resistance, Z_1 and Z_2, the polarisation impedance, computed from (5).

$$Z_{elec} = \left(\frac{1}{R_{ct,elec}} + Q_{elec}(j\omega)^{\alpha_{elec}} \right)^{-1} \tag{5}$$

III. EXPERIMENTAL STUDIES

A. ELECTROLYSER CONFIGURATIONS

The proposed protocol is applied on a commercial electrolyser in two different configurations. A single cell and a 10-cell stack with physical parameters presented in table II. The experiments were carried out on GreenLight E-60 test stations. Each of the proposed phases was repeated at least 10 times during the tests, resulting in a minimum of 1,000 hours of testing for each configuration.

Parameter	Value	Unit
Current density	0.6–2	A/cm^2
Operating pressure H2	0-20	Bar
Operating pressure O2	1 (unpressurised)	atm
Water flow rate	3–60	l/h
Operating temperature	30–70	°C

TABLE II: Main physical characteristics of PEM stack.

Generally, a PEM electrolysis cell consists of several layers assembled under high pressure. These include a $PFSA$ (perfluorosulphonic acid) polymeric membrane, a $Ir/IrO_2/Ru/RuO_2$ supported Ti for anode catalyst, a C supported Pt for cathode catalyst, porous transport layers and bipolar plates in Ti or stainless steel. The above is the configuration of the materials considered in this study.

B. STEADY-STATE PROTOCOL UNDER CURRENT CONTROLLED MODE

The protocol for the two configurations is organized into basic cycles repeated n times until the test time limit or the end-of-test criterion (average voltage deviation of 10% in the I/V curve) is reached. A basic cycle consists of 7 steps, each under constant conditions, with a characterization period (I/V curve and EIS) before and after. A rest period (step 7) allows the electrolyzer to recover most of its reversible losses. At each step, the aim is to activate one or more specific mechanisms:

- Phase 1 (A): nominal conditions, normal degradation.
- Phase 2 (B): effect of temperature, degradation of membrane chains and formation of TiH_2.
- Phase 3 (C): very low frequency start-stop, degradation of the cathode catalyst and reverse current.
- Phase 4 (D): current close to the OCV, formation of HO, degrading the membrane.
- Phase 5 (E): current density greater than $1.5A/cm^2$, $Ir3^+$ formation.
- Phase 6 (F): current density up to $2A/cm^2$, Ti oxidation and TiH_2 formation.
- Phase 7 (R): rest period for reversible losses (catalyst recover and impurities removal).

IV. RESULTS AND DISCUSSIONS

The evolution of the average overpotential (from the I/V curve) and the ohmic and polarisation resistances (from the EIS) are established as the performance indicators for the analysis of accelerated degradation and diagnosis of the electrolyser.

A. ACCELERATED DEGRADATION ANALYSIS THROUGH I/V CURVE

Figures 3 and 4 show the results obtained for the two configurations studied. Last $900h$ for single cell and $1200h$

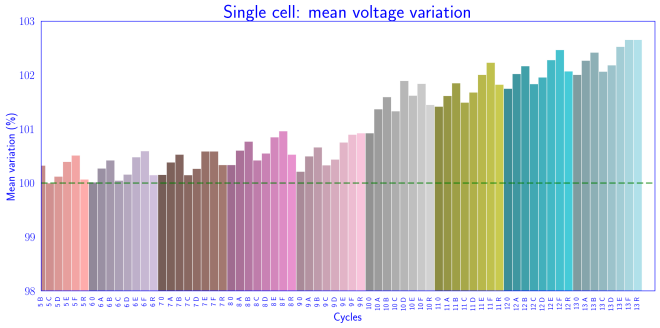

Fig. 3: Mean voltage variation from BoL in the single cell.

for stack.The bar diagram represents the average voltage variation over a range of $0-2\ A/cm$ for the current. This variation is calculated by taking the *BoL* i/V curve as the reference (Step: 0 A). Each colour corresponds to a cycle where a bar represents a step: A,B,C,D,E,F and R (see last section).

All the data correspond to polarisation curves executed in galvanostatic mode. Final voltage variation is 2.7 % for single cell and 2.1 % for stack. With a final variation rate of 36.5 uV/h and 18 $uV/h/cell$, respectively.

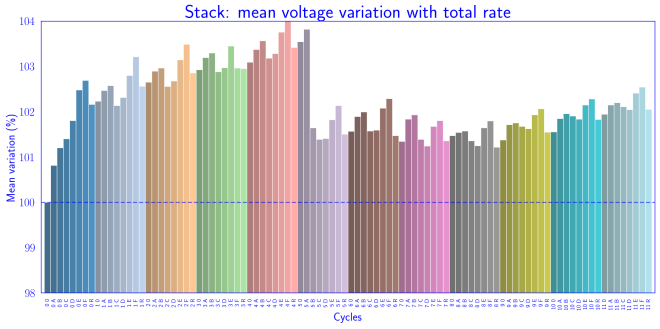

Fig. 4: Mean voltage variation from BoL in the 10-cells stack.

Analysis of the results reveals a number of key points for both configurations:

- The reversible losses are quite noticeable in both configurations, with an average degradation rate of -520 uV/h for the single cell and -769 $uV/h/cell$ for the stack. Reversible losses average 40% and 60% of the average degradation per cycle for each configuration respectively. Their recovery is strongly linked to the resting temperature: moderate temperatures have a greater positive effect on the ageing of the stack. However, the rate of degradation after recovery does not seem to accelerate.
- From phase B, it can see that operating temperature increases degradation at a higher rate than under nominal operating conditions. During this cycle, the measurement of the conductivity of the cathode recirculation water is strongly affected, so that a direct relationship between the cathode catalyst degradation and high temperatures has been established and will be investigated further.
- For both configurations (phase C): single cell and 10-cells stack, start-stop phase help to reduce cell stress and are therefore regenerative, contrary to what was expected from the literature [7]. The cycles are sufficiently long-lasting to allow for a sustained complete shutdown, as well as start-up.
- This last finding also shows a relationship between the duration of the shutdown and the recovery of reversible losses (phase R). Since the regeneration rate of the start-stop and the rest period (of much longer duration) are similar for the single cell. In contrast, the stack seems to require longer recovery periods, as its recovery rate is almost double the start-stop rate.
- Very low current densities (phase D), generally close to the OCV that seeks the formation of *OH* radicals, (degradation of the polymeric membrane), do not seem to have any additional effect to that already generated by temperature. The degradation rates found in phases B and D are similar for the single cell. For the stack, the phase D rate is lower than phase B and seems to decrease with time. The latter is possibly due to the decrease of the current in the stack due to the over-voltage generated by the degradation (galvanostatic control mode).
- Higher current densities are the most degrading for the electrolyser, with a higher hydrogen crossover. The degradation rate of phase F is for each cycle the highest, averaging $460uV/h$ for the single cell and 649 $uV/h/cell$ for the stack.
- However, the degradation rate does not seem to increase proportionally at high ($> 1.5A/cm^2$) and very high ($> 1.8A/cm^2$) current densities. The average degradation rate for phase R (highest current density) is $397uV/h$ for the single cell and 231 $uV/h/cell$ for the stack. Thus, the behaviour of both degradation rates following current density appears to slope steeply at small and moderate magnitude and to stabilise at high currents.

B. ACCELERATED DEGRADATION ANALYSIS THROUGH EIS

The analyses presented below correspond to the EIS data collection performed at 4 measurement points: 20, 40, 400 and 800 mA/cm^2 for each of the steps of the applied protocols. The EIS were carried out in galvanostatic mode under nominal operation conditions. With measurement frequencies between $500Hz$ and $0.05Hz$ for the single cell. The following results correspond to the single cell analysis.

To ensure the quality of the data and to avoid misinterpretation, the Kramers-Kronig test was applied to each of the data sets. For the measurement points of 20 and 40 mA/cm^2 the analysis of the residuals of the applied analytical solution shows that over the whole range of measurement frequencies the residuals do not occupy a region larger than ± 2. For 400 and 800 mA/cm^2 high frequency measurements can go to ± 4. Ideally the literature states a tolerance of $\pm 2\%$ for

a proper interpretation of the data, however, analyses with higher residuals can be applied if previous knowledge of the system is available, to avoid misinterpretation especially in the DRT analysis.

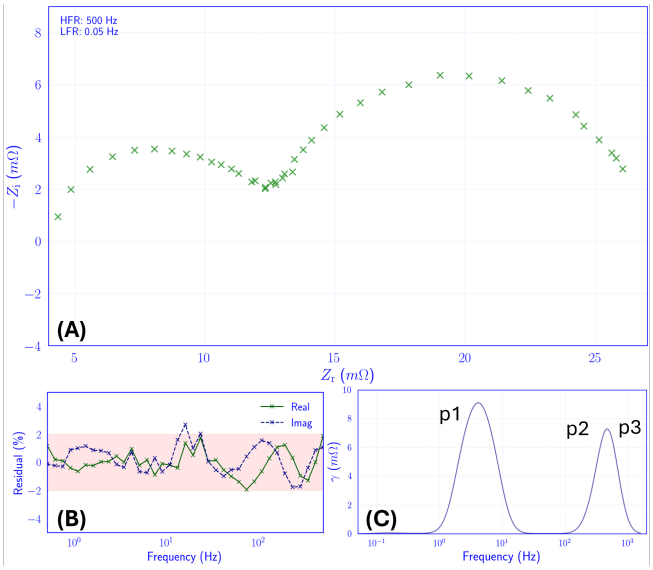

Fig. 5: Analysis of the relaxation times: single cell BoL at 40 mA/cm^2: Nyquist plot (A), Lin-KK test results (B) and decomposed DRT curve with identified peaks (C).

The relaxation time analysis (DRT) applied at the beginning of the tests for the single cell allows the separation of the different electrochemical phenomena according to the characteristic times. From the decomposed DRT curves 3 peaks are identifiable. Figure 5, presents the Nyquist diagram and the DRT results for 40 mA/cm^2. With, $P1$ associated with the first semicircle at low frequencies and $P2+P3$ with the second semicircle at high frequencies. From the analysis by [17], P1 at low frequencies can be associated with the mass transport phenomena, P2 and P3 at high frequencies with the phenomena of activation and charge transport at the electrodes and ionic transport in the membrane, respectively. The polarisation resistance identified are $P1 = 14.6m\Omega$ and $P2+P3 = 6.9m\Omega$ and HF resistance, $R_{HF} = 5.7m\Omega$.

The peaks $P1$, $P2$ and $P3$ evolve according to the current measuring point and the test time, as shown in Figure 6, representing the results for the *DRT* analysis at deferents testing times. In the Nyquist diagrams at different measurement points, it can be seen how the low frequency semicircle contracts, decreasing the area of impedance it comprises, while the semicircle at high frequencies seems to remain constant. $P1$ contracts with increasing frequency as it shifts to the right in the frequency range. $P2+P3$ contract slightly, showing no significant change in the frequency domain. The evolution of the peaks is equally noticeable over time with a slight shift in the frequency range and an increase in the maximum peak of γ.

From the DRT results given in Figure 5 and Figure 6, 3 peaks could be identified, however $P2$ and $P3$ appear to have

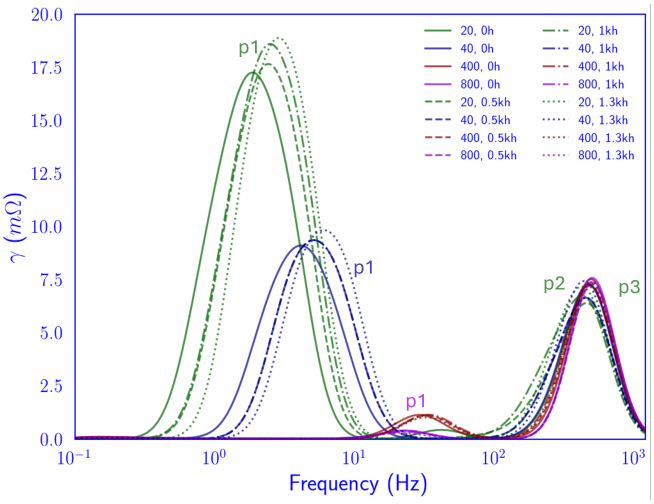

Fig. 6: Deconvoluted DRT peaks of the single cell EIS spectra at 4 measurement point and different testing stages.

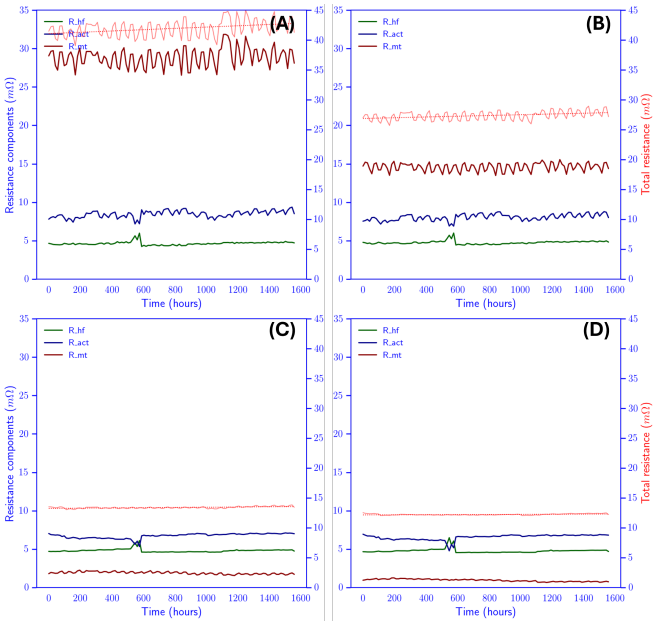

Fig. 7: Evolution of the polarisation resistances at different measurement points for 1.4kh test: 20 (A), 40 (B), 400 (C) and 800 (D) mA/cm^2.

similar relaxation times so that they blend into a single peak at high frequencies. From this analysis it can then be stated that an $R-QR-QR$ *ECM*, such as the one presented in the 2 is relevant. The results obtained for the fitting of the curves of the EIS data present an adequate behaviour to the data and similar to those obtained by the DRT analysis. For the EIS BoL data at $40mAcm^2$, for example, $R_{HF} = 4.8m\Omega$, $R_{act} = 7.6m\Omega$, $R_{mt} = 15.2m\Omega$, corresponding to R_{HF}, $P2+P3$ and $P1$ respectively.

Figure 7 shows the polarisation resistances and HF resistance obtained by fitting the EIS data over the 1.5kh test. As already shown in the DRT analysis, the polarisation resis-

tances decrease considerably with the current measurement point, which also affects the total cell resistance (right axis in the figure). The trend line for the total resistance shows a substantial increase, mostly due to the increase of the R_{HF} and R_{mt}, on average $+4\%$ and $+3\%$, respectively.

V. CONCLUSIONS

The analysis of the polarisation curves is then accurate to evaluate the voltage evolution as an indicator of the general degradation of the electrolyser. Thus, a defined average variation could indicate the end of the experiment or the lifetime of the cell. The operating conditions can also be assessed with respect to the evolution of the over-voltage. In this way a methodological relationship can be established between the operating conditions: temperature, pressure or current density and the technology ageing.

On the other hand, the analysis of the impedance data allows a more precise diagnosis by making it possible to de-combine different electrochemical phenomena linked to proton transport, electrodes charge transport, OER/HER reactions and diffusive phenomena. This precise analysis then allows to link operating conditions and degradation of components and even degradation phenomena if EoL material analyses are performed. This analysis can then be used to determine the state of health of the technology by monitoring the evolution of the internal resistances that ultimately determine the overall performance of the cell and stack.

The analysis of the accelerated degradation of a single cell via the I/V curves and the EIS data then leads to the conclusions in table III. This summary table presents the relative percentage voltage drop (%) and the voltage variation rate in uVh^{-1}, in the second column. The third column reports the behaviour of the inner resistors: increases ($\uparrow$), decreases ($\downarrow$) or no change ($\updownarrow$). Where R_{pol} groups the polarisation resistances.

Phase	**Step mean variation** **I/V curve - (% / uVh^{-1})**	**Polarisation resistances** **EIS**
1 (A)	0.26 / 412	$\updownarrow R_{hf} + \uparrow R_{pol} = \uparrow R_{total}$
2 (B)	0.16 / 253	$\downarrow R_{hf} + \updownarrow R_{pol} = \downarrow R_{total}$
3 (C)	-0.34 / -537	$\uparrow R_{hf} + \downarrow R_{pol} = \downarrow R_{total}$
4 (D)	0.15 / 239	$\downarrow R_{hf} + \downarrow R_{pol} = \downarrow R_{total}$
5 (E)	0.29 / 460	$\uparrow R_{hf} + \uparrow R_{pol} = \uparrow R_{total}$
6 (F)	0.25 / 398	$\updownarrow R_{hf} + \updownarrow R_{pol} = \updownarrow R_{total}$
7 (R)	-0.33 / -521	$\uparrow R_{hf} + \downarrow R_{pol} = \downarrow R_{total}$

TABLE III: Main conclusions from I/V curve and EIS data analysis.

This work has presented the basis of the methodology for the study of the accelerated degradation of a PEM type electrolyser. From the findings of the $3kh$ experiments, some works reported in the literature will been contrasted and discussed. This establishes an experimental basis for the subsequent design and validation of accelerated ageing protocols for large scale application, as the outlook for the coming months of this experimental work.

ACKNOWLEDGMENT

This work has been supported by the EIPHI Graduate School, France (contract ANR-17- EURE-0002) and the Region Bourgogne Franche-Comté.

We gratefully acknowledge the financial support for this work provided by the tyre manufacturer Michelin.

REFERENCES

[1] P. Millet et al., 'PEM water electrolyzers: From electrocatalysis to stack development', International Journal of Hydrogen Energy, vol. 35, no. 10, pp. 5043–5052, May 2010, doi: 10.1016/j.ijhydene.2009.09.015.

[2] M. Chandesris, V. Médeau, N. Guillet, S. Chelghoum, D. Thoby, and F. Fouda-Onana, 'Membrane degradation in PEM water electrolyzer: Numerical modeling and experimental evidence of the influence of temperature and current density', International Journal of Hydrogen Energy, vol. 40, no. 3, pp. 1353–1366, Jan. 2015, doi: 10.1016/j.ijhydene.2014.11.111.

[3] A. Z. Tomić, I. Pivac, and F. Barbir, 'A review of testing procedures for proton exchange membrane electrolyzer degradation', Journal of Power Sources, vol. 557, p. 232569, Feb. 2023, doi: 10.1016/j.jpowsour.2022.232569.

[4] M. Carmo, D. L. Fritz, J. Mergel, and D. Stolten, 'A comprehensive review on PEM water electrolysis', International Journal of Hydrogen Energy, vol. 38, no. 12, pp. 4901–4934, Apr. 2013, doi: 10.1016/j.ijhydene.2013.01.151.

[5] Q. Feng et al., 'A review of proton exchange membrane water electrolysis on degradation mechanisms and mitigation strategies', Journal of Power Sources, vol. 366, pp. 33–55, Oct. 2017, doi: 10.1016/j.jpowsour.2017.09.006.

[6] F. N. Khatib et al., 'Material degradation of components in polymer electrolyte membrane (PEM) electrolytic cell and mitigation mechanisms: A review', Renewable and Sustainable Energy Reviews, vol. 111, pp. 1–14, Sep. 2019, doi: 10.1016/j.rser.2019.05.007.

[7] E. Urbano, E. Pahon, N. Yousfi-Steiner, and M. Guillou, 'Accelerated stress testing in proton exchange membrane water electrolysis - critical review', Journal of Power Sources, 2024, doi: https://doi.org/10.1016/j.jpowsour.2024.235451.

[8] S. Siracusano, S. Trocino, N. Briguglio, V. Baglio, and A. S. Aricò, 'Electrochemical Impedance Spectroscopy as a Diagnostic Tool in Polymer Electrolyte Membrane Electrolysis', 2018.

[9] A. WeiÃŸ, 'Distribution of Relaxation Times Analysis of High-Temperature PEM Fuel Cell Impedance Spectra', Electrochimica Acta, 2017.

[10] D. Brinker, 'Inductive loops in impedance spectra of PEM water electrolyzers', Journal of Power Sources, 2024.

[11] Bernard A. Boukamp 1995 J. Electrochem. Soc. 142 1885

[12] Y. Li, 'Application of distribution of relaxation times method in polymer electrolyte membrane water electrolyzer', Chemical Engineering Journal, 2023.

[13] C. Plank, 'A review on the distribution of relaxation times analysis: A powerful tool for process identification of electrochemical systems', Journal of Power Sources, 2024.

[14] A.N. Tikhonov, A. Gončarskij, V.V. Stepanov, A.G. Jagola (Eds.), Numerical Methods for the Solution of Ill-Posed Problems, Springer, Dordrecht (1995)

[15] M. K. Ratib, 'Electrical circuit modeling of proton exchange membrane electrolyzer: The state-of-the-art, current challenges, and recommendations', i n t e r n a t i o n a l j o u r n a l o f h y d r o g e n e n e r g y.

[16] T.H. Wan, M. Saccoccio, C. Chen, F. Ciucci, Influence of the Discretization Methods on the Distribution of Relaxation Times Deconvolution: Implementing Radial Basis Functions with DRTtools, Electrochimica Acta, 184 (2015) 483-499.

[17] A. Maradesa, B. Py, T.H. Wan, M.B. Effat, F. Ciucci, Selecting the Regularization Parameter in the Distribution of Relaxation Times, Journal of the Electrochemical Society, 170 (2023) 030502.

[18] Ai-Lin Chan, Haoran Yu, Kimberly S. Reeves, Shaun M. Alia, Identifying electrochemical processes by distribution of relaxation times in proton exchange membrane electrolyzers, Journal of Power Sources, Volume 628, 2025.